Fragment isospin distributions and the phase diagram of excited nuclear systems

Ad. R. Raduta
National Institute of Nuclear Physics and Engineering, Bucharest, POB MG6, Romania
(Received 14 April 2005; revised manuscript received 5 July 2005; published 25 January 2006)

Fragment average isospin distributions are investigated within a microcanonical multifragmentation model in different regions of the phase diagram. The results indicate that in the liquid phase $\langle N/Z\rangle$ versus Z is monotonically increasing, in the phase coexistence region it has a rise-and-fall shape, and in the gas phase it is constant. Deviations from this behavior may manifest at low fragment multiplicity as a consequence of mass-charge conservation. Characterization of the "free" and "bound" phase functions of the fragment charge reconfirms the neutron enrichment of the free phase with respect to the bound one irrespectively of the localization of the multifragmentation event in the phase diagram.

DOI: 10.1103/PhysRevC.73.014606 PACS number(s): 24.10.Pa, 25.70.Pq

I. INTRODUCTION

In recent years isospin-dependent phenomena have received much consideration because of their ability to reveal information on the asymmetry term of the nuclear equation of state (EOS). Relying on the fact that, in heavy systems in which the neutron density exceeds the proton density, the asymmetry term is repulsive for neutrons and attractive for protons, theoretical models of heavy-ion reactions predicted different neutron compositions of the liquid and vapor phases [1–6]. More important for studies on EOSs, the difference in the chemical compositions of the gas and liquid phases during a liquid-gas phase transition reflects the magnitude of the asymmetry term and its density dependence. Thus the seminal work of Mueller and Serot [1], which was based on a relativistic mean-field model of nuclear matter with an arbitrary proton fraction, anticipated that it is energetically more favorable for unstable asymmetric nuclear matter to separate into a neutron-rich low-density phase and a neutron-poor high-density one. Later on, the isospin-dependent Boltzmann-Uehling-Uhlenbeck transport model [2], different mean-field approaches [3,4], the antisymmetrized molecular dynamics model [5], the stochastic mean-field model [6], etc., reconfirmed this isospin fractionation phenomenon in both infinite and finite systems. Moreover, to offer a more realistic description of the dynamics of charged asymmetric nuclear matter, Ref. [4] analyzed the effect of the long-range Coulomb interaction, reaching the conclusion that its effect is to diminish the isospin fractionation.

To try to identify this process in experimental multifragmentation data, isoscaling techniques based on grandcanonical assumptions have been applied. The results obtained from reactions involving different combinations of ^{112}Sn and ^{124}Sn at 50 MeV/nucleon bombarding energy [7], $^{112,124}\mathrm{Sn} + {}^{58,64}\mathrm{Ni}$ central collisions at 35 MeV/nucleon [8], multifragmentation reactions induced by high-energy protons [9], and ^{58}Ni, $^{58}\mathrm{Fe} + {}^{58}\mathrm{Ni}$, and ^{58}Fe at 30, 40, and 47 MeV/nucleon [10] proved the expected increase of neutron concentration in the gas phase with respect to the liquid phase.

The aim of this work is to investigate fragment average isospin distributions within a microcanonical multifragmentation model (MMM) that includes in a realistic way the most important ingredients of the nuclear multifragmentation phenomenon and whose phase diagram was studied previously. The advantages of such a study are obvious. First, taking into account that decaying nuclei are small isolated systems, a rigorous statistical treatment requires a microcanonical framework and not an analytically tractable grandcanonical approach. Second, with respect to dynamical models, statistical models have the advantage of dealing with precisely defined fragments. Thus this study is expected to offer a complementary understanding of the problem.

The paper is organized as follows. Section II presents the results obtained within the MMM [11] in three distinct cases: (200, 82) with and without Coulomb interaction and (50, 23) with Coulomb interaction. Fragment average isospin distributions are investigated as functions of fragment charge in each situation. Characteristic shapes of $\langle N/Z\rangle$ versus Z distributions are found in each zone of the phase diagram. Interesting finite-size effects are identified for low multiplicities. Section III investigates the dependence of the above distributions as functions of source isospin. To verify whether the observed signals survive the sequential evaporation stage, effects of the secondary decays are discussed in Sec. IV. To establish a link with dynamical model predictions, an interpretation of the gas and liquid phases with respect to the cluster size is given in Sec. V. Conclusions are drawn in Sec. VI.

II. MICROCANONICAL MULTIFRAGMENTATION MODEL PREDICTIONS

While methods to identify phase transitions in small nonextensive systems accumulate, more importance is given to the fact that, by principle, the most correct statistical approach to be used for exploding nuclei is the microcanonical one [12,13]. In this paper the MMM version [11] of the microcanonical multifragmentation model [13–15] is used.

In this model fragments are placed in a spherical container defining the freeze-out volume. All configurations allowed by mass, charge, total energy, total momentum, and total angular-momentum conservation laws and not forbidden by geometrical constraints (overlapping between fragments or

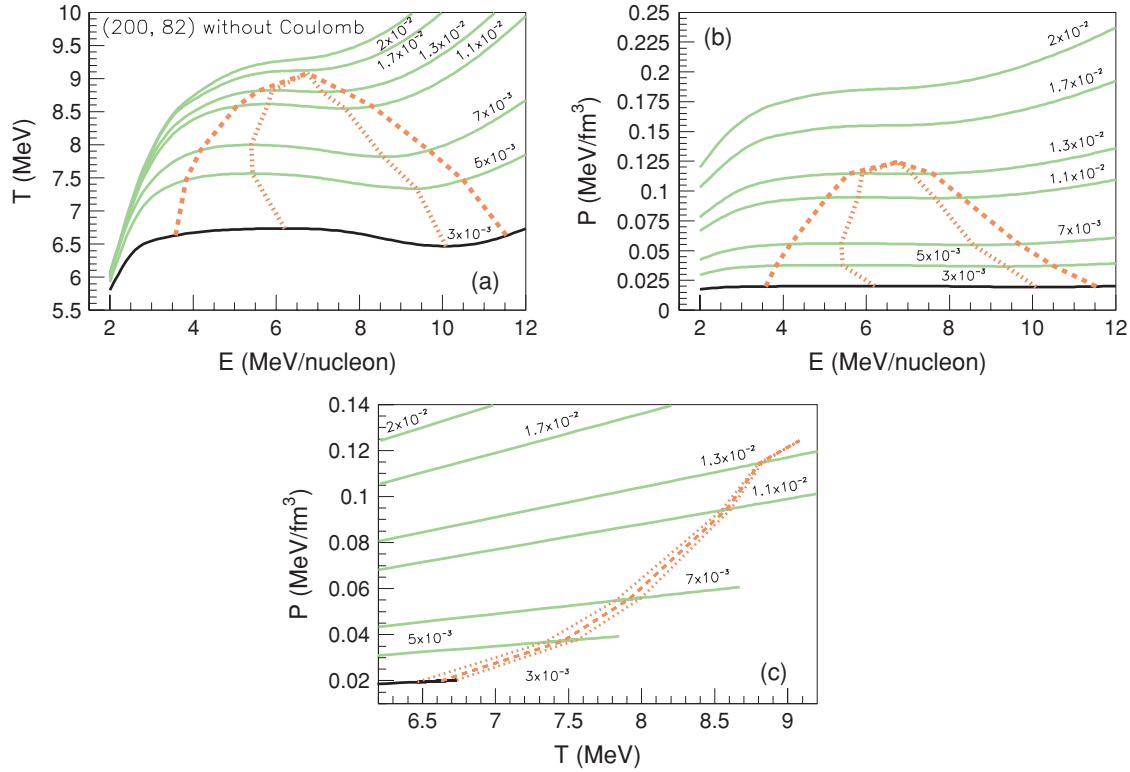

FIG. 1. (Color online) Phase diagram of a (200, 82) nuclear system without Coulomb and hard-core interactions in (a) temperature-excitation energy (b) pressure-excitation energy, and (c) pressure-temperature representations. The solid curves correspond to the considered iso-βP trajectories; the dashed curves indicate the borders of the phase-coexistence region; and the dotted curves indicate the borders of the spinodal region. The βP values of the iso-βP curves are labeled in units of inverse cubic femtometers.

with container's walls) are spanned by a Metropolis Monte Carlo trajectory in the configuration space. The key quantity of the model is the weight of each configuration, which has a nonanalytically tractable form and enters the expression of any physical observable. The breakup fragments relevant for thermodynamics may be excited highly enough to deexcite by sequential particle emission. If not explicitly mentioned otherwise, this paper focuses on the breakup stage of the reaction, but for the sake of completeness a brief discussion of effects of secondary decays is included.

Depending on whether fragments are assimilated with (i) hard nonoverlapping spheres or (ii) normal nuclear density malleable objects, one may distinguish two freeze-out cases. Even if, for a given state of the statistically equilibrated source characterized by the mass, charge, excitation energy and freeze-out volume, the two cases may lead to different results, the thermodynamics associated to the model is qualitatively the same. Freeze-out case (ii) has the important advantage of allowing the system to reach high densities, being thus preferable when one aims to investigate the phase diagram.

While realistic by their microcanonical foundation, statistical multifragmentation models may be criticized because of the too simplistic treatment of the freeze-out volume. Indeed, it is hard to imagine that fragment production into a vacuum takes place in a fixed-size spherical box, but rather in a volume fluctuating from event to event and characterized by it average value. Statistical models used the fixed-volume hypothesis in order to diminish, presumably without significant consequences, the dimension of the configuration space. More recent works [16] suggest treating the multifragmenting nucleus in a modified microcanonical ensemble in which the volume is allowed to fluctuate and the microcanonical weight of a configuration $W(E, V)$ is multiplied by $\exp(-\beta P V)$ (where β is the inverse temperature and P is a pressure), the average value of the volume being determined by its Lagrange multiplier βP.

The fact that in the case of time-dependent open systems the thermodynamical definition of volume is still an open problem is illustrated by the different concepts presently employed. Thus dynamical models define the freeze-out volume by the spatial extension of the system when fragments cease to interact with each other otherwise than by the Coulomb field, implying thus a minimum distance of 2–3 fm between them. A somehow similar image in the sense that volume does not act as an external constraint corresponds to the dynamical models that define the freeze-out volume with respect to the freeze-out time, a notion that assumes chemical equilibrium: Fragments can still exchange nucleons, but their multiplicity has to be time independent. Maybe one of the most illustrative examples of what freeze-out volume may mean within dynamical models, in contrast to the statistical ones, is given by the recent study of Ref. [17]. Here the authors show that the freeze-out volume depends dramatically on freeze-out instant and fragment multiplicity. As the message

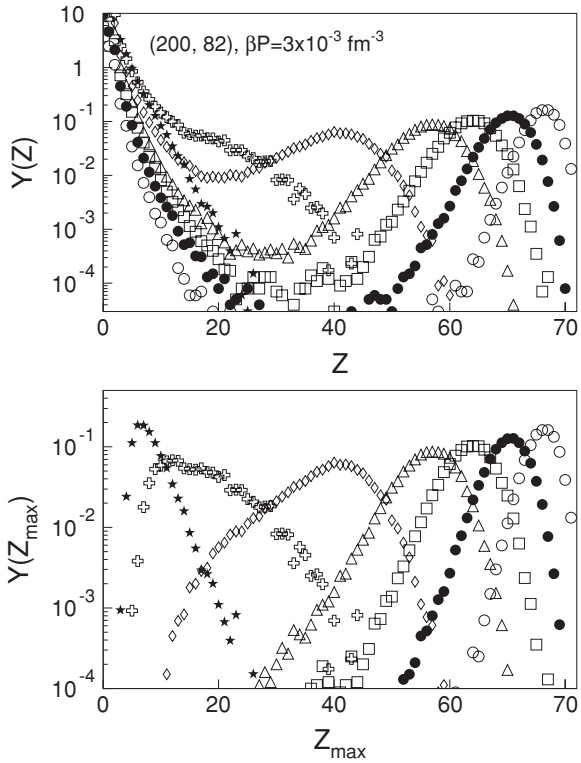

FIG. 2. (Top) fragment charge distributions and (bottom) charge distributions of the largest fragment for the (200, 82) nuclear system without Coulomb interaction at different excitation energies. For all considered situations the system in constrained by $\beta P = 3 \times 10^{-3}$ fm^{-3}. The key legend is as follows: open circles, $E = 3$ MeV/nucleon; filled circles, $E = 4$ MeV/nucleon; open squares, $E = 5$ MeV/nucleon; open triangles, $E = 6$ MeV/nucleon; open diamonds, $E = 8$ MeV/nucleon; crosses, $E = 10$ MeV/nucleon, stars, $E = 12$ MeV/nucleon.

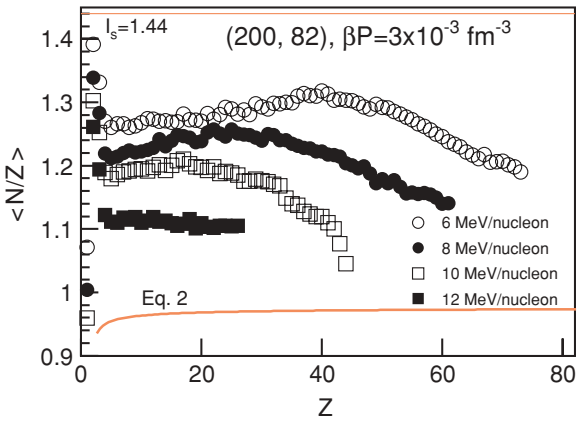

FIG. 3. (Color online) Fragment average isospin distributions as functions of fragment charge for the (200, 82) nuclear system without Coulomb interaction at different excitation energies. For all considered situations the system in constrained by $\beta P = 3 \times 10^{-3}$ fm^{-3}. The horizontal line indicates the source's isospin, $I_s = 1.44$. The thick solid curve corresponds to the most probable isospin value obtained from the liquid-drop formula of the binding energy, Eq. (2).

of this paper relies on the thermodynamical characterization of the nuclear system, it is stressed here that, in the case of the MMM, the volume is even more than an unphysical fictitious container that obliges the *preformed* fragments not to separate, but dictates also their partition as the volume enters the statistical weight of a configuration. Apart the obvious explicit dependence, the volume acts by means of the thermal kinetic energy defined as the difference between the total available energy (input quantity) and all other partial energies (internal excitation, Coulomb interaction, and fragment formation Q).

The phase diagram associated with the MMM was studied in Refs. [18,19], and the conclusions must be underlined. For small systems, like (50, 23), irrespective of whether the Coulomb interaction is present or not, the system evolves from the liquid phase present at low excitation energies to the gas phase corresponding to vaporized matter by crossing the coexistence zone. For large systems, like (200, 82), which experience stronger Coulomb fields, the situation becomes more interesting. When one turns the Coulomb interaction off, the system exhibits the same behavior as that of a small system. When the Coulomb field is activated, the critical temperature and pressure decrease such that, for freeze-out volumes up to about $100V_0$, the system may evolve from the liquid phase to gas or supercritical fluid without crossing the phase-coexistence zone [19].

In the following subsections the MMM predictions of fragment average isospin distributions at different points of the nuclear phase diagram are presented, and the fact that $\langle N/Z \rangle$ versus Z manifests different behavior in the liquid, phase-coexistence, and gas regions is stressed. As a general comment, it is mentioned that the investigation of the phase space along constant βP paths is arbitrary and the description of the system within a modified microcanonical ensemble with fluctuating volume [16] is not essential for the conclusions of the present study. Thus the same behavior of $\langle N/Z \rangle$ versus Z distributions determined by the event localization inside the phase diagram was obtained for constant-volume approximation (standard microcanonical approach).

A. (200, 82) without Coulomb interaction

The phase diagram of the nuclear system (200, 82) without Coulomb and hard-core interactions [freeze-out case (ii)] is shown in Fig. 1 in the temperature-excitation energy, pressure-excitation energy, and pressure-temperature planes. The solid curves represent iso-βP trajectories for different values of βP ranging from 3×10^{-3} to 2×10^{-2} fm^{-3}, as indicated in the figure. The borders of the phase-coexistence region were evaluated by use of a Maxwell construction on the iso-βP caloric curves and are plotted with dashed curves. The borders of the spinodal region are defined as the locus of the inflexion points of $T(E)|_{\beta P}$ curves and are plotted with dotted curves. The critical point is characterized by the following set of values: $T_C = 9.1$ MeV, $P_C = 1.25 \times 10^{-1}$ MeV/fm^3, $E_C = 6.75$ MeV/nucleon, and $(V/V_0)_C = 1.33$.

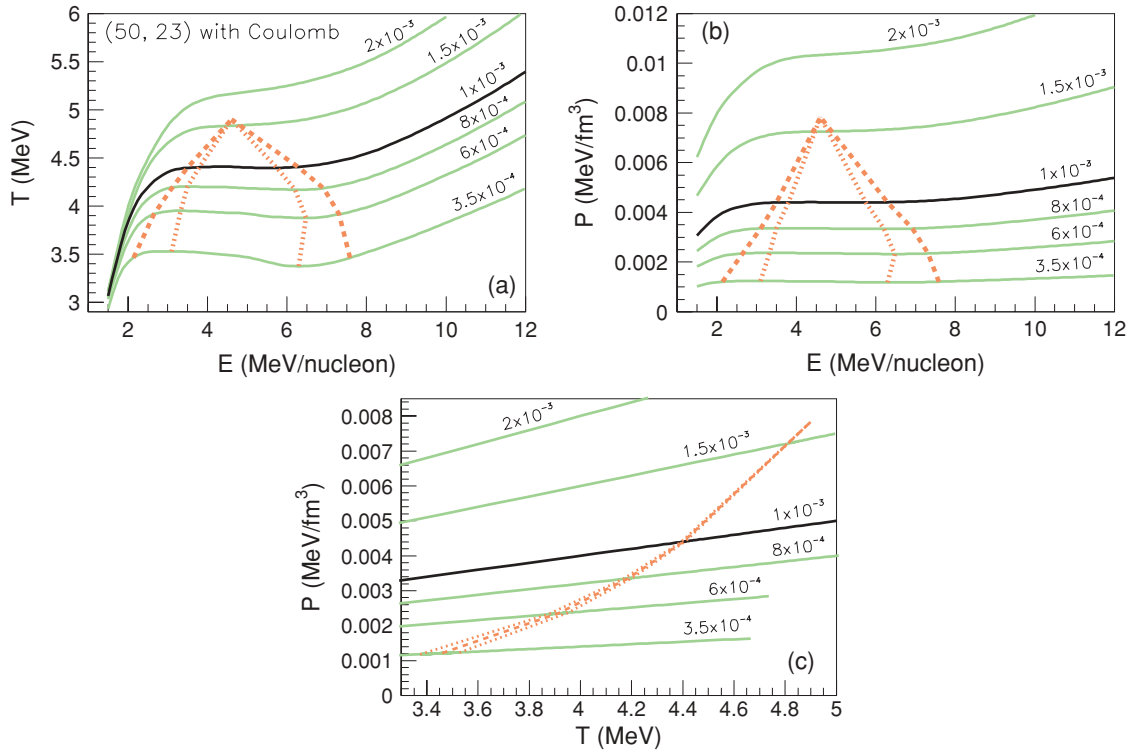

FIG. 4. (Color online) Phase diagram of a (50, 23) nuclear system with Coulomb interaction and free-volume parametrization in (a) temperature-excitation energy, (b) pressure-excitation energy, and (c) pressure-temperature representations. The solid curves correspond to the considered iso-βP trajectories; the dashed curves indicate the borders of the phase-coexistence region; and the dotted curves indicate the borders of the spinodal region. The βP values of the iso-βP curves are labeled in units of inverse cubic femtometers.

The shapes of $\langle N/Z \rangle$ versus Z distributions have been investigated along all iso-βP paths shown in Fig. 1. To illustrate the conclusions, the phase space is scanned along the trajectory characterized by $\beta P = 3 \times 10^{-3}$ fm^{-3}. The states obtained in this way are similar to the ones obtained in nuclear multifragmentation reactions. Thus, as the excitation energy increases from 2 to 12 MeV/nucleon, the temperature range is around 6 MeV and the average freeze-out volume increases linearly from 2 V_0 to 16 V_0.

Once the thermodynamical behavior of the system is clarified and before the fragment average isospin distributions are investigated as functions of fragment size, it is useful to have a clear picture of the fragment size distributions produced in the considered multifragmentation events. Figure 2 shows the fragment charge distributions (upper panel) and charge distributions of the largest fragment in each event (lower panel).

Even if our main purpose for plotting $Y(Z)$ is only to illustrate the fragment charge population for each state of the source, the correct information on event localization in the phase diagram we may get in this case from the shape of $Y(Z)$ distributions is remarkable. Thus, as one may note from the upper panel of Fig. 2, as far as the system consists of liquid + undersaturated vapor ($E = 3.6$–1.5 MeV/nucleon) $Y(Z)$ has a U or a shoulderlike shape, whereas it falls exponentially in the supersaturated vapor phase ($E > 11.5$ MeV/nucleon), as anticipated in the early days of multifragmentation [13–15]. This result is all the more striking as it does not hold for the case in which the Coulomb interaction is strong, as one may see in the next subsection.

The decision to investigate how $Y(Z_{\max})$ distributions look is motivated by the fact that the largest fragment is expected to be an order parameter of the phase transition [20] and a good estimation of the liquid phase [21]. The information emerging from the lower panel of Fig. 2 is that, when the excitation energy is increased, the centroid of the $Y(Z_{\max})$ distribution shifts toward lower values while its shape evolves in a complicated manner. Thus, despite the coexistence region, for $E = 4$, 5, and 6 MeV/nucleon, $Y(Z_{\max})$ is single peaked and symmetric enough to hinder any information on the true localization of the event in the phase diagram of the system. For higher excitation energies, $E = 8$, 10 MeV/nucleon, the $Y(Z_{\max})$ distributions become broad and asymmetric such that one may interpret their shapes as the result of the superposition of two Gaussian distributions corresponding to each phase of the system. For this short energy interval the information extracted from $Y(Z_{\max})$ distributions is correct. For excitation energies higher than 11.5 MeV/nucleon, the system consists of supersaturated vapor, the $Y(Z)$ distribution has an exponential decrease, the largest residual nucleus has on average fewer than 10 protons, and the $Y(Z_{\max})$ distribution is single peaked and narrow. For this case the information inferred from $Y(Z_{\max})$ is again correct. The limited and not always correct information the largest cluster distribution may provide on localization of multifragmentation events in the phase diagram has recently been studied within a lattice gas model [22] and

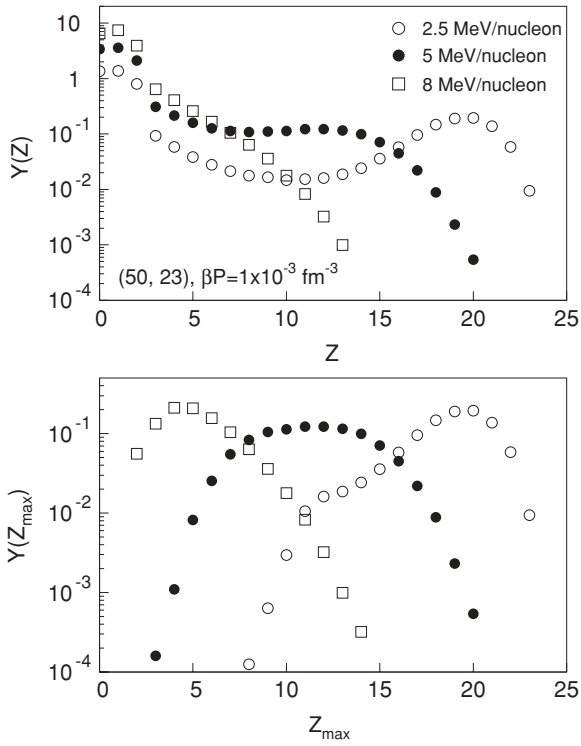

FIG. 5. (Top) Fragment charge distributions and (bottom) charge distributions of the largest fragment for the (50, 23) nuclear system with Coulomb interaction at different excitation energies. For all considered situations the system in constrained by $\beta P = 1 \times 10^{-3}$ fm^{-3}.

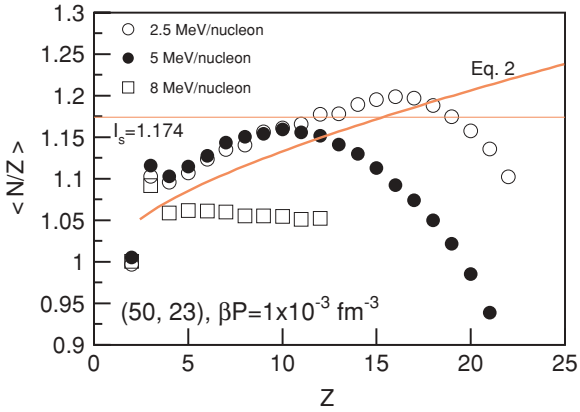

FIG. 6. (Color online) Fragment average isospin distributions as functions of fragment charge for the (50, 23) nuclear system with Coulomb interaction in the liquid ($E = 2.5$ MeV/nucleon), liquid-gas coexistence ($E = 5$ MeV/nucleon) and gas phase ($E = 8$ MeV/nucleon) regions. For all considered situations the system in constrained by $\beta P = 1 \times 10^{-3}$ fm^{-3}. The horizontal line indicates the source's isospin, $I_s = 1.174$. The thick solid curves corresponds to the most probable isospin value obtained from the liquid-drop formula of the binding energy, Eq. (2).

explained as a consequence of mass and charge conservation in microcanonical and canonical ensembles.

Figure 3 shows the fragment average isospin ($\langle N/Z \rangle$) distributions as functions of fragment charge for the above-considered excitation energies. Setting apart the average isospin of light charged particles ($Z < 5$) strongly affected by structure effects, one may observe that, in the coexistence region, $\langle N/Z \rangle$ versus Z manifests a clear rise-and-fall behavior and in the supersaturated vapor phase it is constant. Moreover, in the coexistence region the average isospin of a fragment belonging to the liquid is monotonically decreasing with its charge.

The occurrence of the liquid + undersaturated vapor phase at low values of excitation energy and/or freeze-out volume prevents fragment production in the intermediate-size domain ($15 < Z < 30$), as evidenced in Fig. 2 by the $Y(Z)$ distribution corresponding to $E = 3$ MeV/nucleon. Moreover, the small values of the total fragment multiplicity make the isospin of clusters whose size is close to the source size sensitive to mass and charge conservation. For these reasons, it was not possible to obtain conclusive $\langle N/Z \rangle$ versus Z distributions.

The effect of excitation energy on $\langle N/Z \rangle$ versus Z distributions within a given region of the phase diagram is quite trivial. Thus, when the excitation energy is increased, the number of emitted neutrons increases such that, for conserving the mass and charge of the total system, the isospin of the rest of matter is decreasing, leading to the observed shift of $\langle N/Z \rangle$ versus Z distributions toward lower values. The decrease of the turning point where the rising distribution starts to decrease may be understood if one keeps in mind the diminishing of the liquid part with the increase in the excitation energy.

B. (50, 23) with Coulomb interaction

To verify whether the obtained results stand valid while modifying the system size and switching the Coulomb interaction on, in the following discussion we investigate another system, (50, 23) with Coulomb interaction.

The phase diagram obtained with freeze-out case (ii) is shown in Fig. 4 in the temperature-excitation energy, pressure-excitation energy, and pressure-temperature planes. As in the previous case, the solid curves represent iso-βP trajectories for different values of βP ranging from 3.5×10^{-4} to 2×10^{-3} fm^{-3}, as indicated in the figure. The borders of the phase coexistence (dashed curves) and the spinodal (dotted curves) regions are determined as in Subsec. II. A. The critical point is characterized by the following set of values: $T_C = 4.9$ MeV, $P_C = 7.8 \times 10^{-3}$ MeV/fm^3, $E_C = 4.6$ MeV/nucleon, and $(V/V_0)_C = 12$. The striking difference between the coordinates of this critical point and the one corresponding to the (200, 82) without the Coulomb interaction case is not only a finite-size effect, but mainly the consequence of including the Coulomb interaction. Thus, even for a relatively small system like the (50, 23) nucleus, the Coulomb field is strong enough to force the system to occupy a large volume and to diminish in this way the repulsive effect. If true, a critical volume of about 12 V_0 would imply that real nuclear multifragmentation reactions for which the freeze-out volume was estimated to be 3–9 V_0 take place at supercritical values.

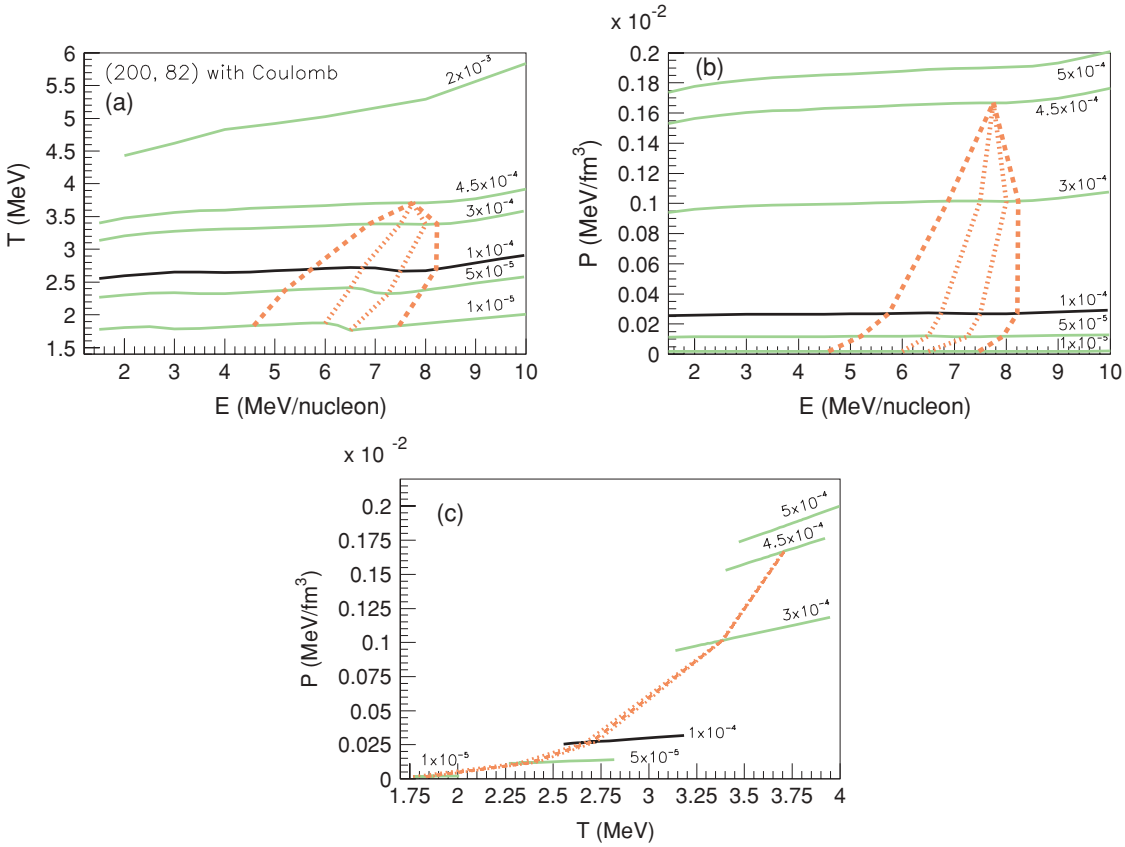

FIG. 7. (Color online) Phase diagram of (200, 82) nuclear system with Coulomb interaction and free-volume parametrization in (a) temperature-excitation energy (b) pressure-excitation energy, and (c) pressure-temperature representations. The solid curves correspond to the considered iso-βP trajectories; the dashed curves indicate the borders of the phase-coexistence region; the dotted curves indicate the borders of the spinodal region. The βP values of the iso-βP curves are labeled in units of inverse cubic femtometers.

As in the previous case, to illustrate the behavior of fragment average isospin distributions in the liquid, phase-coexistence, and gas regions we follow a constant $\beta P = 1 \times 10^{-3}$ fm^{-3} path. As one may see in Fig. 4, along the considered trajectory the system consists of a liquid with an undersaturated vapor for $E \leqslant 3.5$ MeV/nucleon; for 3.5 MeV/nucleon $\leqslant E \leqslant 6.3$ MeV/nucleon, the system undergoes phase separation into a liquid and its associated saturated vapor; and for $E > 6.3$ MeV/nucleon the system is a supersaturated vapor. For complete thermodynamical information on the explored states, have it should be mentioned that the excitation energy increase from 1.5 to 8 MeV/nucleon leads to a linear increase of the average freeze-out volume from 10 V_0 to 50 V_0.

Fragment charge distributions and charge distributions of the largest fragment are plotted in Fig. 5. As in the previous case, the localization of multifragmentation events in the phase space is correctly indicated by the shape of the $Y(Z)$ distributions: Up to 3.5 MeV/nucleon, $Y(Z)$ has a U shape; for $3.5 < E < 6$ MeV/nucleon, $Y(Z)$ has a shoulderlike shape; and for $E > 6.5$ MeV/nucleon, $Y(Z)$ is falling exponentially. Regarding the $Y(Z_{\max})$ distributions, the small size of the system makes the mass-charge conservation effects stronger than those observed for the (200, 82) nucleus. Indeed, the $Y(Z_{\max})$ distributions corresponding to 2.5 and 8 MeV/nucleon are truncated and no bimodality or any particular structure that may suggest superposition of close distributions corresponding to different phases can be identified for 5 MeV/nucleon excitation energy. The only effect that may suggest in this last case a particular state of the system is the rather broad $Y(Z_{\max})$ distribution. In addition, for $E = 2.5$ MeV/nucleon, the competition between evaporationlike decay and multifragmentation induces a hump in the $Y(Z_{\max})$ distribution that could be interpreted as bimodality and erroneously associated with phase coexistence.

Figure 6 shows $\langle N/Z \rangle$ versus Z distributions that correspond to the liquid, liquid-gas, and gas phases of the (50, 23) system. For the coexistence region ($E = 5$ MeV/nucleon) and for the gas phase ($E = 8$ MeV/nucleon) the shapes look like the ones obtained for the (200, 82) nucleus; in the phase-coexistence region $\langle N/Z \rangle$ versus Z has a rise-and-fall shape; and for the gas phase it is almost constant. A striking result is the one corresponding to 2.5 MeV/nucleon, which seems to be compatible with the phase-coexistence region. The explanation of this apparent paradox lies in the fact that for such a small system and low excitation energies the total fragment multiplicity is around 3, meaning that each emitted light particle will modify drastically the isospin of the residual nucleus. Thus the observed rise and fall is a consequence of mass and charge conservation.

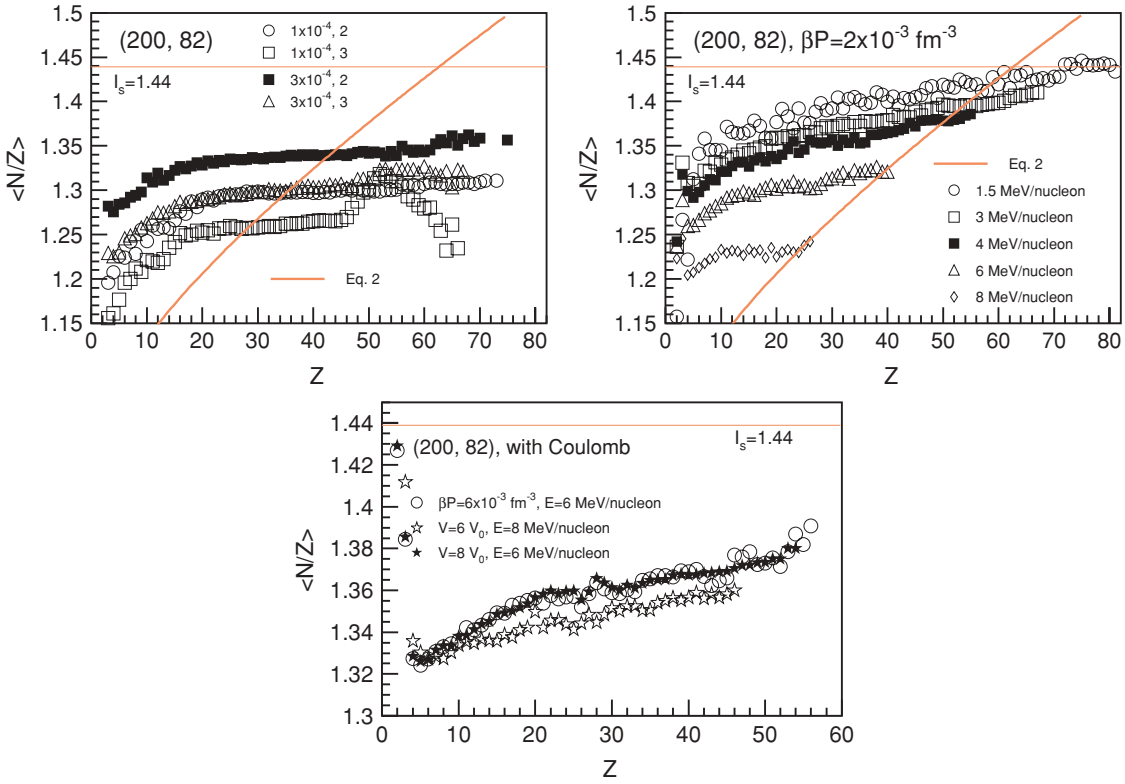

FIG. 8. (Color online) Fragment average isospin distributions as functions of fragment charge for the (200, 82) nuclear system with Coulomb interaction. Upper-left-hand panel, liquid + undersaturated vapor phase for $\beta P = 1 \times 10^{-4}$ and 3×10^{-4} fm^{-3}, $E = 2$, 3 MeV/nucleon; upper-right-hand panel, supercritical fluid phase along $\beta P = 2 \times 10^{-3}$ fm^{-3}; lower panel, freeze-out case (i) and different freeze-out volume approximations as indicated in the figure. The horizontal line indicates the source's isospin, $I_s = 1.44$. The thick solid curve corresponds to predictions of Eq. (2).

C. (200, 82) with Coulomb interaction

The system's expansion into volumes much larger than those estimated for multifragmentation reactions under the repulsive effect of the Coulomb field is expected to increase with the system size. This fact is confirmed by the phase diagram of the (200, 82) excited nucleus plotted in Fig. 7 in temperature-excitation energy, pressure-excitation energy, and pressure-temperature representations. The critical point is characterized by $T_C = 3.7$ MeV, $P_C = 1.7 \times 10^{-3}$ MeV/fm^3, $E_C = 7.75$ MeV/nucleon, and $(V/V_0)_C = 130$, and phase coexistence occurs for freeze-out volumes of at least a few hundred V_0.

Even if not interesting for nuclear multifragmentation, the iso-βP trajectories plotted in Fig. 7 offer the possibility of investigating the liquid phase without the undesired effects of low fragment multiplicity. The upper-left-hand panel of Fig. 8 depicts the typical monotonic increase of $\langle N/Z \rangle$ versus Z distributions in different states of the liquid + undersaturated vapor system ($\beta P = 1 \times 10^{-4}$ fm^{-3}, $E = 2$ MeV/nucleon, and $\beta P = 3 \times 10^{-4}$ fm^{-3}, $E = 2, 3$ MeV/nucleon). Deviations from this shape may be due to mass-charge conservation, as one may see for $\beta P = 1 \times 10^{-4}$ fm^{-3} and $E = 3$ MeV/nucleon case in which the hump present around $Z = 50$ is produced by the dominant fissionlike decay. Thermodynamical states more similar to those produced in multifragmentation reactions are obtained along the supercritical $\beta P = 2 \times 10^{-3}$ fm^{-3} path where the freeze-out volume increases linearly from 4 V_0 (for $E = 1.5$ MeV/nucleon) to 30 V_0 (for $E = 8$ MeV/nucleon). The corresponding average isospin distributions plotted in the upper-right-hand panel of Fig. 8 show the same monotonic increase as that observed for the liquid phase. It is worthwhile mentioning here that an $\langle N/Z \rangle$ increasing with Z was reported by other microcanonical models [23] and experimental data obtained in deep inelastic collisions of Kr and Nb [24].

The lower panel of Fig. 8 presents some extra fragment average isospin distributions corresponding to the same (200, 82) with the Coulomb system under freeze-out case (i) and different freeze-out volume approximations: (1) constant $\beta P = 6 \times 10^{-3}$ fm^{-3} and $E = 6$ MeV/nucleon ($\langle V \rangle = 8.08\ V_0$, $T = 6.88$ MeV), (2) constant $V = 6V_0$ and $E = 8$ MeV/nucleon ($T = 7.68$ MeV), and (3) constant $V = 8V_0$ and $E = 6$ MeV/nucleon ($T = 6.90$ MeV). The first and the third cases were chosen so as to be characterized by almost identical values of the (average) freeze-out volume, excitation energy, and temperature but differing by the freeze-out volume approximation: In the first case, the volume is fluctuating, whereas in the last one it is fixed. The monotonic increase of $\langle N/Z \rangle$ versus Z distributions obtained in all cases and the almost perfect superposition between the

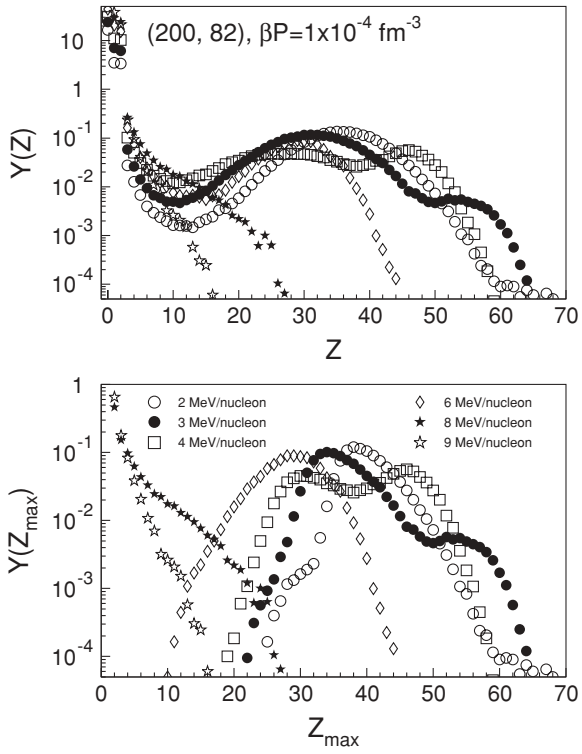

FIG. 9. (Top) Fragment charge distributions and (bottom) charge distributions of the largest fragment for the (200, 82) nuclear system with Coulomb interaction at different excitation energies. For all considered situations the system in constrained by $\beta P = 1 \times 10^{-4}$ fm^{-3}.

isospin distributions obtained in (1) and (3) illustrate that the presented results do not depend on the freeze-out volume approximation.

Regarding the evolution of $\langle N/Z \rangle$ versus Z with increasing excitation energy, the comments done in the previous section stand valid, namely that when the number of emitted neutrons is increased, the isospin of the rest of the system decreases, leading to the observed shift of $\langle N/Z \rangle$ versus Z distributions.

New examples on how misleading fragment charge distribution may be when one is dealing with microcanonical approaches are provided by the same $\beta P = 1 \times 10^{-4}$ fm^{-3} path and are plotted in Fig. 9. Thus, for the lowest considered excitation energy, 2 MeV/nucleon, the system consists of liquid and undersaturated vapor, whereas the shoulderlike shape of the $Y(Z)$ distribution and the asymmetric shape of the $Y(Z_{\max})$ distribution would suggest liquid-saturated vapor coexistence. For 3 and 4 MeV/nucleon, the situation is even more difficult: The presence of fission as a decay mechanism induces a W shape of the $Y(Z)$ distributions and a bimodal structure of the $Y(Z_{\max})$ distributions that could be erroneously interpreted as a signature of phase coexistence. When the system enters the liquid-saturated vapor state, the situation is again tricky: For 6 MeV/nucleon, the $Y(Z_{\max})$ distribution is single-peaked. The high-energy border of the phase-coexistence region (8 MeV/nucleon) is characterized by a shoulderlike shape of both the $Y(Z)$ and the $Y(Z_{\max})$ distributions. In the supersaturated vapor phase, $Y(Z)$ and $Y(Z_{\max})$ fall exponentially, giving

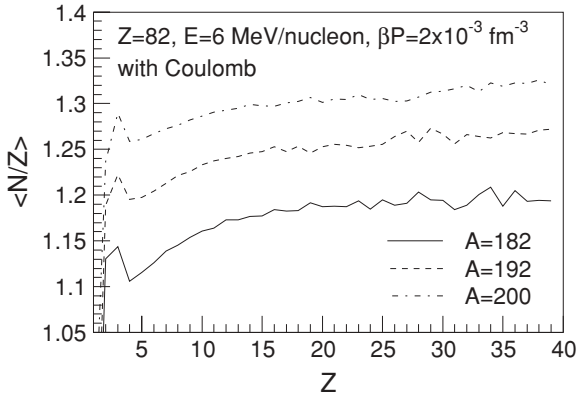

FIG. 10. Fragment average isospin distributions corresponding to three sources characterized by $Z = 82$ and $A = 182$, 192, and 200 with excitation energy 6 MeV/nucleon and $\beta P = 2 \times 10^{-3}$ fm^{-3}. For all cases Coulomb and hard-core interactions are considered.

for the first time correct information on the localization of the multifragmentation event in the phase space.

To understand whether the obtained behavior of the fragment average isospin distributions is caused by the specific fragment partition in different regions of phase space or is a trivial consequence of the liquid-drop binding energy,

$$B(A,Z) = a_v \left[1 - a_i \left(1 - \frac{2Z}{A}\right)^2\right] A - a_s \left[1 - a_i \left(1 - \frac{2Z}{A}\right)^2\right] A^{2/3} - a_c Z^2 A^{-1/3} + a_a Z^2/A, \quad (1)$$

one may calculate the most probable value of a fragment isospin as a function of its mass (charge) by requiring that $\partial B/\partial I|_A = 0$. In the present simulation, $a_v = 15.4941$ MeV, $a_s = 17.9439$ MeV, $a_i = 1.7826$, $a_c = 0.7053$ MeV, and $a_a = 1.1530$ MeV [25].

By solving this equation, one obtains for the most probable isospin,

$$I(A) = 1 + \frac{a_c A^{5/3} - a_a A}{2a_i(a_v A - a_s A^{2/3})}, \quad (2)$$

a function that is monotonically increasing with fragment size, irrespective of whether $a_c = 0$ (the Coulomb interaction is switched off) or not. The corresponding isospin distributions as a function of Z obtained with Eq. (2) are plotted in Figs. 3, 6, and 8. Thus the only situation for which we obtain qualitative agreement between the MMM fragment average isospin distributions and predictions of the liquid-drop binding energy corresponds to the liquid + undersaturated vapor state of the system. However, it is not generally true that the liquid phase of nuclear matter is characterized by a monotonic increase of the average isospin as a function of fragment size because, when the system is in liquid + saturated vapor coexistence, the largest fragment in each event that definitely belongs to the liquid part does not show the same behavior. Thus, taking into account that, in the heavy-fragment

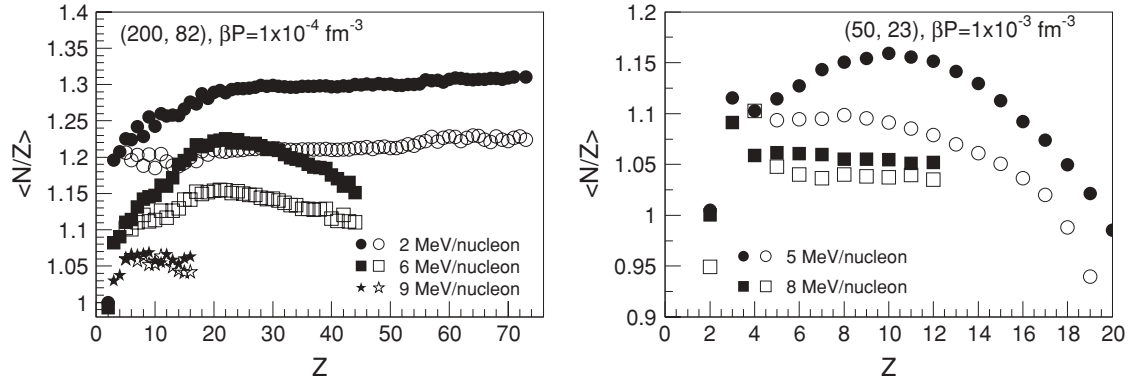

FIG. 11. Fragment average isospin distributions in the breakup (filled symbols) and asymptotic (open symbols) stages of the reaction. The left-hand panel corresponds to the case of (200, 82) nucleus, $\beta P = 1 \times 10^{-4}$ fm^{-3} with $E = 2$, 6, and 9 MeV/nucleon; the right-hand panel corresponds to the case of (50, 23) nucleus, $\beta P = 1 \times 10^{-3}$ fm^{-3} with $E = 5$, 8 MeV/nucleon. In all cases the Coulomb interaction is present. Freeze-out case (ii) was used.

range of the mass spectrum (where $\langle N/Z \rangle$ decreases with Z) the dominant fragment is the largest one in each event, we easily anticipate the fall of the average isospin of the largest cluster with its size. This means that, at least within the currently used MMM, fragment partition at breakup does not obey a total symmetry energy minimization principle but is the consequence of the interplay of all observables entering the statistical weight of a configuration—the key quantity of the model.

III. EFFECT OF SOURCE ISOSPIN ON $\langle N/Z \rangle$ VERSUS Z DISTRIBUTIONS

To provide a more complete picture on how sensitive the average isospin distributions are with respect to the isospin of the source nucleus, $\langle N/Z \rangle$ versus Z distributions were analyzed in different regions of the phase diagram. Because the results are similar irrespective of the position of the multifragmentation event inside the phase diagram, only the most physically relevant case of a source with $Z = 82$ with Coulomb interaction whose mass number was varied from 182 to 200 is presented. Here, freeze-out case (i) was used. Thus Fig. 10 illustrates $\langle N/Z \rangle$ versus Z distributions obtained for the excitation energy 6 MeV/nucleon and $\beta P = 2 \times 10^{-3}$ fm^{-3}. The result is intuitive: When the source isospin is increased, more neutrons are emitted at breakup and all produced fragments are more neutron rich, leading to a shift of the $\langle N/Z \rangle$ versus Z distributions toward higher values of N/Z without any noticeable modification of their shape.

IV. EFFECT OF SECONDARY PARTICLE EVAPORATION

Even if all thermodynamical relevant information corresponds to the breakup stage of the reaction, in the following discussion we analyze the effect of secondary particle emission from primary excited fragments. The motivation is that this reaction stage is the one accessible in multifragmentation experiments. Sequential particle emission is treated by use

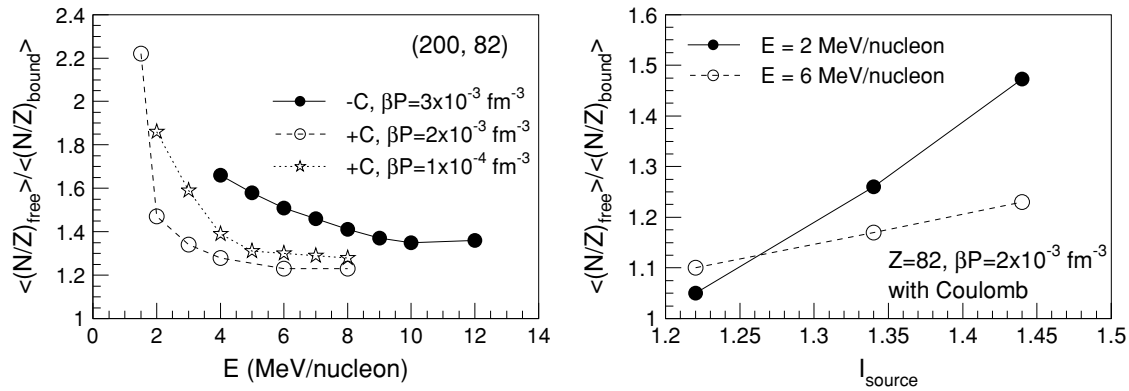

FIG. 12. Left-hand panel, relative neutron enrichment of the "free" phase with respect to the "bound" phase for the (200, 82) nuclear system with and without the Coulomb interaction when the associated phase spaces are explored following the βP constant paths 2×10^{-3} and 1×10^{-4} fm^{-3} (with the Coulomb interaction) and 3×10^{-3} fm^{-3} (without the Coulomb interaction); right panel, Relative neutron enrichment of the "free" phase with respect to the "bound" phase as a function of the source's isospin in the case of a system with $Z = 82$, with Coulomb interaction at 2 and 6 MeV/nucleon excitation energy and $\beta P = 2 \times 10^{-3}$ fm^{-3}.

of the standard Weisskopf evaporation scheme as described in Ref. [11].

Given that during the evaporation stage neutrons are emitted with the largest probability, one may expect a more symmetric matter in the asymptotic stage of the reaction with respect to the breakup stage. However, the dependence of evaporation probabilities on both fragment average excitation energy and isospin makes the evaporation effect difficult to anticipate quantitatively and raises the question of whether isospin distributions observed in the breakup stage survive in the asymptotic stage of the reaction. To answer this question, Fig. 11 illustrates the results obtained at different points of the phase diagram in the physical case in which the Coulomb interaction is present. The liquid + undersaturated vapor phase is represented by (200, 82) with $\beta P = 1 \times 10^{-4}$ fm^{-3} and $E = 2$ MeV/nucleon; the liquid + saturated vapor coexistence is represented by (200, 82), $\beta P = 1 \times 10^{-4}$ fm^{-3}, and $E = 6$ MeV/nucleon and (50, 23), $\beta P = 1 \times 10^{-3}$ fm^{-3}, $E = 5$ MeV/nucleon; the supersaturated vapor phase is represented by (200, 82) with $\beta P = 1 \times 10^{-4}$ fm^{-3}, $E = 9$ MeV/nucleon and (50, 23), $\beta P = 1 \times 10^{-3}$ fm^{-3}, $E = 8$ MeV/nucleon. The conclusions are that, for the liquid phase, particle evaporation induces a lowering of the fragment average isospin without modifying the linear dependence of $\langle N/Z \rangle$ on Z. For the phase-coexistence region, sequential evaporations act such that the rise-and-fall shape of $\langle N/Z \rangle$ versus Z is diminished without being washed out. This effect is easy to understand if one keep in mind that the neutron emission is stronger for the neutron-rich fragments (maximum of $\langle N/Z \rangle$ versus Z) with respect to the neutron-poor fragments from the extremities of $\langle N/Z \rangle$ versus Z distribution. The breakup fragments that form the supersaturated vapor phase are almost symmetric, such that sequential particle emission does not change to a significant extent their isotopic composition. The asymptotic stage average isospin values corresponding to light charged particles ($Z < 4$) have been omitted from Fig. 11 because of the presence of some irregularities that can be interpreted as artefacts of the simplified procedure by which secondary decays have been implemented [11].

V. DO WE HAVE ISOSPIN FRACTIONATION IN STATISTICAL MULTIFRAGMENTATION MODELS?

Because isospin fractionation was decided by both dynamical models and experimental multifragmentation data analyzing exclusively the isotopic content of light charged emitted clusters, it would be interesting to check to what extent our predictions agree with the reported results. To make this comparison straightforward, I adopt one of the methods applied by the dynamical models and classify the fragments as parts of liquid and gas phases according to their mass. Thus, in the spirit of Ref. [5], here it is assumed that the collection of fragments with $Z \leqslant 4$ form the "free" phase and the rest of fragments form the "bound" phase. I prefer to call the obtained subsystems "free" instead of "gas" and "bound" instead of "liquid" because the above-mentioned classification may be done irrespectively of the localization of the multifragmentation event in the phase diagram, even outside the phase-coexistence region. The choice of $Z = 4$ as criterion for phase definition is arbitrary, and similar results have been obtained when $Z = 2$ has been used.

The left-hand panel of Fig. 12 shows the relative neutron enrichment of the "free" phase with respect to the "bound" phase for the (200, 82) nuclear system with (without) Coulomb interaction along the $\beta P = 2 \times 10^{-3}$ and 1×10^{-4} fm^{-3} (3×10^{-3} fm^{-3}) constant paths. As one may see, for all considered cases $\langle N/Z \rangle_{\text{free}} / \langle N/Z \rangle_{\text{bound}}$ is larger than 1, meaning that isospin distillation takes place and that its exact values depend on the observables characterizing the state of the source. It is mentioned at this point that relative neutron enrichment of the free phase that decreased with increasing energy was evidenced also by dynamical models [2], a quantitative comparison is nevertheless impossible because of different definitions of phases.

The right-hand panel of Fig.12 shows the dependence of the relative enrichment of the "free" phase as a function of source isospin. As expected, the more isospin asymmetric the initial system, the more neutron rich the corresponding "free" phase obtained by multifragmentations. Similar linear behavior was reported by dynamical models [2].

An important remark to be made is that, at least in the framework of the currently used MMM, the neutron enrichment of the "free" phase with respect to the "bound" phase is not necessarily connected with phase coexistence because it manifests even for the (200, 82) with Coulomb interaction case in which, for freeze-out volumes smaller than several tens of V_0, the employed model does not enter the phase-coexistence region (left-panel of Fig. 12).

VI. CONCLUSIONS

Fragment isospin distributions have been investigated with-in the framework of MMM. The obtained distributions manifest different shapes in the liquid, liquid-gas, and gas regions of the phase diagram. For small systems with low excitation energies, mass and charge conservation constraints modify the shape of $\langle N/Z \rangle$ versus Z distributions from one that monotonically increases to one that has a maximum. Distributions of the largest fragment in each event expected to be a good order parameter of the phase transition and a reliable estimation of the liquid part do not manifest bimodality in the whole phase-coexistence zone and confirm the conclusions of Ref. [22], which state that mass conservation induces modifications of the $Y(Z_{\max})$ distributions from the one obtained in infinite systems. Moreover, for low excitation energies, $Y(Z_{\max})$ shows bimodality outside the coexistence region because of the interplay between evaporation and fission as decay mechanisms. Isospin fractionation is found to be compatible with a microcanonical multifragmentation case, and effects of secondary particle emission and isospin of the source are investigated. Phase classification according to the cluster size proves that neutron enrichment of the "free" phase with respect to the "bound" one depends on the source state. Finally, neutron enrichment of the "free" phase is not a signal of phase coexistence since it is observed everywhere in the phase space.

[1] H. Muller and B. D. Serot, Phys. Rev. C **52**, 2072 (1995).
[2] B.-A. Li, Phys. Rev. Lett. **85**, 4221 (2000).
[3] T. Sil, S. K. Samaddar, J. N. De, and S. Shlomo, Phys. Rev. C **69**, 014602 (2004).
[4] S. J. Lee and A. Z. Mekjian, Phys. Rev. C **68**, 014608 (2003).
[5] A. Ono, P. Danielewicz, W. A. Friedman, W. G. Lynch, and M. B. Tsang, Phys. Rev. C **68**, 051601(R) (2003).
[6] V. Baran, M. Colonna, M. Di Toro, V. Greco, M. Zielinska-Pfabe, and H. H. Wolter, Nucl. Phys. **A703**, 603 (2002).
[7] H. S. Xu *et al*., Phys. Rev. Lett. **85**, 716 (2000).
[8] E. Geraci *et al*., Nucl. Phys. **A732**, 173 (2004).
[9] E. Martin, R. Laforest, E. Ramakrishnan, D. J. Rowland, A. Ruangma, E. M. Winchester, and S. J. Yennello, Phys. Rev. C **62**, 027601 (2000).
[10] D. V. Shetty, S. J. Yennello, E. Martin, A. Keksis, and G. Souliotis, Phys. Rev. C **68**, 021602(R) (2003).
[11] Al. H. Raduta and Ad. R. Raduta, Phys. Rev. C **55**, 1344 (1997); **65**, 054610 (2002).
[12] D. H. E. Gross and M. E. Madjet, cond-mat/9611192, submitted to Phys. Rev. Lett.
[13] D. H. E. Gross, Rep. Progr. Phys. **53**, 605 (1990).
[14] J. P. Bondorf, A. S. Botvina, A. S. Iljinov, I. N. Mishustin, and K. Sneppen, Phys. Rep. **257**, 133 (1995).
[15] S. E. Koonin and J. Randrup, Nucl. Phys. **A474**, 173 (1987).
[16] F. Gulminelli, Ph. Chomaz, and V. Duflot, Europhys. Lett. **50**, 434 (2000).
[17] M. Parlog *et al*., Eur. Phys. J. A **25**, 223 (2005).
[18] Al. H. Raduta and Ad. R. Raduta, Phys. Rev. Lett. **87**, 202701 (2001).
[19] F. Gulminelli, Ph. Chomaz, Al. H. Raduta, and Ad. R. Raduta, Phys. Rev. Lett. **91**, 202701 (2003).
[20] X. Campi, J. Desbois, and E. Lipparini, Phys. Lett. **B138**, 353 (1984).
[21] J. B. Elliott *et al*., Phys. Rev. C **62**, 064603 (2000).
[22] F. Gulminelli and Ph. Chomaz, Phys. Rev. C **71**, 054607 (2005).
[23] D. V. Shetty, A. S. Botvina, S. J. Yennello, A. Keksis, E. Martin, and G. A. Souliotis, nucl-ex/0401012.
[24] G. A. Souliotis, D. V. Shetty, M. Veselsky, G. Chubarian, L. Trache, A. Keksis, E. Martin, and S. J. Yennello, Phys. Rev. C **68**, 024605 (2003).
[25] W. D. Myers and W. J. Swiatecki, Nucl. Phys. **81**, 1 (1967); Ark. Fys. **36**, 343 (1967).